Research Square

Preprints are preliminary reports that have not undergone peer review.
They should not be considered conclusive, used to inform clinical practice,
or referenced by the media as validated information.

# Representation-dependent transportability of single-cell-derived myeloid- and fibroblast/stromal-associated transcriptional programs in bladder cancer

**Mingran Zhang**
Department of Urology, The Third Affiliated Hospital of Soochow University
**You Zhao**
Department of Urology, The Affiliated Liyang People's Hospital of Kangda College of Nanjing Medical University
**Hongzhao Ma**
mhz202608@163.com

**Research Article**

**Keywords:** bladder cancer, single-cell RNA sequencing, transcriptional programs, transportability, reproducibility, tumor microenvironment, spatial transcriptomics, bioinformatics

**Posted Date:** November 1st, 2026

**DOI:** https://doi.org/10.21203/rs.3.rs-11050428/v1

**License:** This work is licensed under a Creative Commons Attribution 4.0 International License.
Read Full License

**Additional Declarations:** No competing interests reported.

# Abstract

Single-cell-derived transcriptional programs are often transported to bulk and external single-cell datasets. It remains unclear, however, at which representation level these programs remain informative. We evaluated four eligible myeloid–stromal program pairs derived from exploratory single-cell analyses of bladder cancer across multiple external cohorts and data types.

We tested locked 30-gene programs in TCGA-BLCA, GSE13507 and GSE31684, in the external scRNA-seq datasets GSE222315 and GSE301651, and in 22 spatial sections from GSE319536. Bulk associations were assessed by Spearman correlation. In the external scRNA-seq datasets, we examined lineage representation, fixed clustering and state matching, Harmony sensitivity, patient-wise leave-one-gene-out (LOO) coherence, and expression-matched null controls. Fixed-marker tissue-composition adjustment, spatial depth sensitivity and clinical associations were examined as secondary analyses.

All 12 bulk pair-by-cohort correlations were positive (Spearman rho 0.585–0.851). However, results across the full 2 × 2 set of eligible pairs did not support a unique interpretation for any one pair. In the external scRNA-seq datasets, lineage-level patient coverage was complete, but direction agreement and top-20 marker overlap were weak for discrete-state matching. Patient-wise LOO coherence was positive at the dataset level and exceeded expression-matched null expectations. Rescoring with common genes had little effect on bulk correlations (absolute change ≤ 0.020). Fixed-marker composition adjustment substantially reduced these correlations. Spatial within-section co-variation was weak after depth adjustment and was sensitive to filtering. Section-level spatial autocorrelation was also low. Clinical associations varied across analyses, and none of the overall-survival associations was significant.

Transportability depended on the representation level. Fixed programs retained detectable within-lineage coherence across external datasets, but this did not show preservation of discrete states, a specific myeloid–stromal axis, or a cellular interaction.


# Introduction

Bladder cancer is heterogeneous at both the molecular and histological levels. Bulk transcriptomic data therefore contain signals from malignant, immune, and stromal cells at the same time [1]. Single-cell studies have shown this heterogeneity in more detail and identified different epithelial, myeloid, and fibroblast-associated transcriptional patterns in bladder tumors [2–5]. These cell-state-related gene programs can also be tested in other datasets. However, their meaning depends on the type of data being analyzed. In bulk tissue, for example, a high program score may partly reflect differences in cell composition. A gene set may also remain coherent within a lineage without reproducing the same discrete cell state in another cohort.

Myeloid and stromal programs are a useful example. Macrophage-associated transcriptional programs have been linked to inflammatory and immunoregulatory features of the bladder-cancer microenvironment [2, 6]. Macrophage-associated states are heterogeneous across tumor contexts [7, 8].

Fibroblast-associated programs often reflect extracellular-matrix production and tissue remodeling, both of which are common features of tumor stroma [4, 9]. Myeloid and stromal signals may therefore vary together across tumors. Their scores can also become strongly correlated in bulk tissue. Such a correlation, however, does not identify the cells responsible for the pattern or show that the two cell populations interact. Several bulk signatures have also been associated with clinical features in selected cohorts [9–12], although mixed cell composition makes their biological interpretation less specific.

Single-cell data allow these programs to be examined within a defined lineage. A fixed gene set can be tested to see whether its genes still vary together across individual patients. Recovering the original discrete state is more difficult. Clustering depends on sampling, patient composition, integration, and other analysis choices. The original cluster may therefore not reappear even when part of its transcriptional pattern is still present. Conversely, a continuous within-lineage relationship is not enough to claim that the same discrete state has been reproduced.

Spatial profiling provides tissue-location information, but its interpretation also has limits. Many spatial spots contain more than one cell type, and score associations can be affected by spatial resolution, sequencing depth, filtering, and the analytical framework [13–17]. We therefore used bulk, single-cell, and spatial data to address different questions rather than treating them as equivalent validation approaches.

Bulk analysis was used to test whether program scores varied together across tumors. In single-cell data, we examined whether the genes in each program remained coherent within the relevant lineage and across individual patients. We assessed discrete state matching separately, based on agreement in differential-expression patterns and marker structure. Spatial analysis was used to test whether program scores co-varied within tissue sections. Keeping these analyses separate was important because each captures a different level of the signal.

In this study, we examined a fixed exploratory set of bladder-cancer gene programs across several data types. The discovery analysis generated eight locked 30-gene programs. Two were myeloid-associated and two were fibroblast/stromal-associated. These four programs defined the complete 2 × 2 set of eligible myeloid–fibroblast pairs used in the present post-selection analysis. All four pairs were tested. We did not select only the strongest one.

We first tested bulk co-variation across independent cohorts. We then examined the external scRNA-seq datasets in two ways: discrete state-level matching and continuous patient-wise, within-lineage leave-one-out (LOO) coherence. Matched random gene sets were analyzed with the same procedure to determine whether the observed coherence was greater than expected for expression-matched genes. We also tested the effect of program-gene composition, estimated tissue composition, within-section spatial co-variation, and secondary clinical features.

This study was a post-selection evaluation of a fixed exploratory program set. The external scRNA-seq and spatial datasets were used to test how well these programs carried across datasets and

measurement types. They were not prospective confirmatory validation cohorts.

# Materials and Methods

### Study Design and Evidence Boundary

The discovery-state inventory and the eight 30-gene program definitions were generated in an exploratory single-cell workflow. The discovery input comprised eight public GSE135337 gene-by-cell UMI tables (42,823 raw cells; 42,430 cells after project quality control). Matrices were processed with Seurat 5.5.1 [18] using log normalization with a scale factor of 10,000, selection of 2,000 VST variable features, scaling and PCA with 30 principal components. Harmony [19] used sample as the grouping variable; neighbors used dimensions 1–20 with k = 20, followed by Seurat algorithm 1 clustering at resolution 0.5 with random seed 1. The state-QC framework marked single-sample states and states dominated by one sample among at most two samples as FAIL; states with dominant-sample fraction >0.6 among more samples were CONDITIONAL; stress-signature and unannotated states were LOW. Thus, 50 candidate discovery states were evaluated under the recorded state-QC framework rather than all being assumed to have passed QC. The locked 2 × 2 pair universe for the present study comprised Mac_TRM and Mac_IFN crossed with Fib_7 and Fib_8. Bulk cohorts contributed to the post-selection cross-cohort evaluation history. GSE222315, GSE301651 and GSE319536 were introduced after pair-focus selection for external transportability analyses and were not prospective confirmatory validation cohorts. No program was added, deleted or reselected according to an external result.

### Discovery scRNA-seq Processing, State Review and Program Definition

GSE135337 comprised BC1–BC7 primary-tumor samples and a BCN paracancerous sample from BC4. After lineage-specific subclustering, 50 GSE135337 discovery states were evaluated against 18 GSE169379 validation states. Because one patient contributed both BC4 and BCN, state representation and dominance are sample-level quantities. Exploratory cross-dataset comparison with GSE169379 used lineage-internal state matching based on expression correlation together with top-20 marker overlap and Jaccard similarity. A state was retained when expression correlation exceeded 0.25 or top-20 marker Jaccard exceeded 0.05; these thresholds were exploratory pipeline choices and were not documented as prespecified confirmatory criteria. The eight retained states were represented by fixed 30-gene programs. The program-construction script used the first 30 lineage-internal markers; only when fewer than 10 lineage-internal markers were available did it use the first 30 corresponding versus-all markers. All eight locked outputs contained exactly 30 genes. The 30-gene lists were locked downstream definitions; the top-20 marker lists were a separate matching metric and were not substituted for program definitions.

### Bulk Preprocessing, Scoring and Cross-Cohort Evaluation

The locked 30-gene definitions were applied without further modification. Program scoring was identical in logic across platforms and adapted only to input scale. For TCGA-BLCA, the processed symbol-

collapsed expression matrix was used; duplicated gene symbols were collapsed with the locked rowsum rule. For GSE13507 and GSE31684, deposited normalized log-expression matrices were used with locked platform-specific probe-to-symbol mappings; when multiple probes mapped to one gene, the probe with the highest median expression across samples was retained. Within each bulk cohort, per-gene z-scores were calculated across samples after removing zero-variance rows, and each program score was the mean of the standardized values for locked genes present on that platform. Pairwise associations were assessed with Spearman correlation using complete observations (two-sided; exact = FALSE). Bootstrap 95% confidence intervals and Benjamini–Hochberg adjustment were applied to the 12 pair-by-cohort evaluations. For the fixed-marker paired bootstrap, subjects were resampled with replacement, the fixed composition proxies and fully adjusted pair correlations were recalculated within each replicate, and the statistic was adjusted rho(Mac_TRM, Fib_8) minus adjusted rho(Mac_IFN, Fib_8). Ten thousand iterations used seed 20260817; percentile 95% confidence intervals and the fraction of replicates with a positive difference were retained.

**Program-Gene Robustness Analyses**

For common-gene sensitivity, each program was rescored using genes shared by the relevant bulk platforms and compared with the original fixed-program score. Locked marker-removal sensitivities removed CLEC9A, IL2RA, SLC12A5 and HLA-DQA2 from Mac_TRM for the Mac_TRM × Fib_8 analysis, and TYROBP, SRGN and LYZ from Fib_7 for the two Fib_7-containing analyses. These were sensitivity analyses of fixed definitions; they did not create revised state labels.

**External scRNA-seq QC, Lineage Annotation and State Matching**

GSE222315 used the locked QC thresholds nFeature_RNA ≥200 and ≤7,500 with percent.mt ≤20; P1_BCa through P9_BCa tumor samples were retained and NAT samples were excluded. GSE301651 used nFeature_RNA >200 and <10,000 with percent.mt <40. Eleven independent primary bladder-tumor patients were retained after excluding lymph-node and peripheral-blood samples and mapping repeated material to patients rather than counting it as independent patients. Major lineages were assigned independently of the target programs using canonical marker panels for myeloid/macrophage, fibroblast/stromal, epithelial, T/NK, B/plasma and endothelial compartments.

For GSE222315, canonical marker panels were: myeloid/macrophage (LST1, TYROBP, FCER1G, CTSS, AIF1, LILRB1, C1QA, C1QB, C1QC, CD68, CD163, FOLR2, MRC1, MS4A7); fibroblast/stromal (COL1A1, COL1A2, COL3A1, DCN, LUM, COL6A1, COL6A2, COL6A3, PDGFRA, COL5A1, COL5A2, C7); epithelial (EPCAM, KRT8, KRT18, KRT19, KRT5, KRT14, KRT17, KRT7, UPK1A, UPK2, UPK3A); T/NK (CD3D, CD3E, TRBC1, TRBC2, IL7R, LTB, NKG7, GNLY, KLRD1, CD8A); B/plasma (CD79A, MS4A1, CD37, CD74, HLA-DRA, CD79B, JCHAIN, MZB1, IGKC, CD19); and endothelial (EMCN, PECAM1, VWF, KDR, ENG, ESAM, RAMP2, PLVAP). For GSE301651, the corresponding panels were: myeloid/macrophage (LYZ, LST1, FCER1G, TYROBP, CTSS, AIF1, CST3); fibroblast/stromal (COL1A1, COL1A2, DCN, LUM, COL3A1, PDGFRA, COL6A1); epithelial (EPCAM, KRT8, KRT18, KRT19, KRT7, KRT17, KRT14); T/NK (CD3D, CD3E, TRBC1, TRBC2, IL7R, NKG7, GNLY); B/plasma (CD79A, MS4A1, CD74, HLA-DRA, CD37, MZB1, JCHAIN); and

endothelial (PECAM1, VWF, EMCN, KDR, ESAM, RAMP2, ENG). The locked target programs did not guide major-lineage annotation.

Within myeloid/macrophage and fibroblast/stromal lineages, one fixed primary clustering specification was used: 30 principal components were calculated; a 20-nearest-neighbor graph used PCs 1–20; Seurat algorithm 1 clustering used resolution 0.5 and random seed 1. Locked-program matching was evaluated as the best candidate cluster versus the remaining cells of the same lineage. For each candidate cluster, the signed effect was the mean log1p library-size-normalized expression in that cluster minus the corresponding mean in the remaining cells of the same lineage, evaluated over finite comparable locked genes. The best cluster maximized the Pearson correlation between the external signed-effect vector and the original locked-state effect vector. Because this correlation was maximized over candidate clusters, it is selection-conditioned and was treated as a descriptive matching metric rather than an independent replication statistic. Matching summaries therefore jointly considered finite comparable genes, same-direction genes, signed effects, signed effect correlation, shared top-20 markers and Jaccard overlap. Missing or non-estimable values were retained as NA/NE and not converted to zero. No resolution search, alternative integration-method search or outcome-driven parameter selection was performed.

**Harmony Sensitivity**

Harmony used patient ID as the only grouping variable. Within each dataset and major lineage, log-normalization used scale factor 10,000; 2,000 VST variable features were selected and scaled; 30 PCs were calculated; Harmony was run on PCA dimensions 1–30; and neighbors/clustering used Harmony dimensions 1–20, k = 20, algorithm 1, resolution 0.5 and seed 1. Exactly one Harmony clustering was run per dataset and lineage. Pre- and post-Harmony results were compared for dominant-patient fraction, direction fraction, signed effect correlation and top-20 overlap.

**Cluster-Free LOO Coherence and Matched-Null Analysis**

External coherence was evaluated separately within each patient and appropriate lineage. Expression was residualized per gene across cells against an intercept, log1p(nCount_RNA), nFeature_RNA and percent.mt when available. Residuals were z-standardized per gene across cells. Missing or zero-variance genes were non-comparable and were never filled with zero. For each comparable gene g, the LOO score excluded g itself and was the mean residual z-score of the other comparable program genes. Spearman rho between g and its LOO score was calculated across cells. Gene-level rho values were summarized by their median within each patient and program; dataset-level values were the median of patient-level summaries. Patients were the biological replication unit, and no cell-level P value was used as replication evidence.

For matched-null analysis, 1,000 expression-matched random gene sets were sampled for each patient-program combination with seed 20260910. Eligible null genes were detectable and non-zero-variance genes from the same patient and lineage, matched by expression decile with adjacent-bin fallback; sets

contained no duplicate genes and excluded observed program genes. The identical residualization, z-standardization and LOO calculation was applied to observed and null sets. Patient-level observed summaries were compared with their own null distributions, and dataset-level summaries were medians across patients.

### Fixed-Marker Composition Sensitivity

Estimated epithelial, macrophage and fibroblast/stromal composition scores used fixed marker panels. The epithelial panel was EPCAM, KRT5, KRT20, UPK1B and KRT13; the macrophage panel was LYZ, CD14, CD68, C1QC, FCGR3A and CSF1R; and the fibroblast/stromal panel was GREM1, COL12A1, POSTN, VCAN, COL1A2, PDLIM3, COL6A3, CALD1, INHBA and SULF1. Program-pair correlations were compared before and after adjustment for these estimated composition scores using the locked rank-residual partial-Spearman correlation procedure, with epithelial, macrophage and fibroblast/stromal proxy scores as covariates. The marker-based scores were used as sensitivity proxies rather than as a definitive cell-fraction estimate, in the context of existing expression-based abundance methods [20–23]. A paired bootstrap (10,000 iterations; seed 20260817) evaluated within-cohort differences in fixed-marker-adjusted residual correlations for Mac_TRM × Fib_8 and Mac_IFN × Fib_8. Program–macrophage-proxy correlations were reported to show collinearity relevant to residual interpretation.

### Spatial Analysis

GSE319536 was analyzed as 22 sections from 22 patients [24]. Count-based spatial matrices were library-normalized per 10,000 and log1p-transformed. Within each section, per-gene z-scores were calculated and each locked program score was the mean standardized value across program genes present; the section was the inferential unit. The primary recoverable QC threshold was UMI ≥200, with threshold sensitivity at UMI ≥500 and UMI ≥1,000. Raw and depth/detection-adjusted within-section Spearman correlations were summarized across sections. Depth-adjusted correlations used the locked rank-residual partial-Spearman procedure with log1p(total spot UMI) and detected-gene count as covariates. Moran's I used native Visium adjacency. At UMI ≥200, 85,347 spots were retained; the deposited in-tissue count was 103,011, whereas a previously published manually filtered count of 70,575 could not be reproduced because the manual spot barcode list was unavailable. The within-section 75th percentile of the Mac_TRM score was calculated, and sections with q75 >0.2 were counted at each UMI threshold as a historical descriptive detectability threshold, not as biological validation.

### Clinical Analysis, Software and Reproducibility

Clinical comparisons were treated as secondary phenotype analyses. Two-group comparisons used two-sided Wilcoxon rank-sum tests with Cliff's delta and the locked alphabetical group order; positive values indicate higher scores in group_1 and negative values indicate higher scores in group_2. Five estimable clinical comparisons per program entered the specified Benjamini–Hochberg multiplicity family. Overall survival was evaluated with univariable Cox proportional-hazards models as secondary context and was not interpreted as prognostic evidence when non-significant. Analysis scripts and audit tables preserved

fixed inputs, intermediate summaries and final reported values. The recorded computational environment used R 4.6.0, Seurat 5.5.1, harmony 2.0.5, Matrix 1.7.5 and data.table 1.18.4.

# Results

### Exploratory program definition and the complete tested universe

GSE135337 included eight samples from seven patients, including paired tumor and paracancerous samples from one patient; 50 candidate discovery states were identified, and discovery-state representation was therefore summarized at the sample level. An exploratory lineage-internal comparison with GSE169379 used expression-correlation and top-20-marker Jaccard criteria [25]. Eight states met the exploratory retention rule of expression correlation >0.25 or top-20 marker Jaccard >0.05 and were represented by fixed 30-gene programs (Figure 1A,B).

The present analysis used the locked 2 × 2 pair universe composed of Mac_TRM and Mac_IFN, each paired with Fib_7 and Fib_8. Thus, four pairs were examined: Mac_TRM × Fib_7, Mac_IFN × Fib_7, Mac_TRM × Fib_8 and Mac_IFN × Fib_8 (Figure 1C). Fib_7 was retained as an identity-confounded comparator; it was not interpreted as a validated fibroblast state. The program definitions and pair universe were fixed before the analyses reported below.

### Bulk cross-cohort co-variation is reproducible across the locked 2 × 2 pair universe

All four program pairs showed positive Spearman correlations in all three bulk cohorts (Figure 2A,B). For Mac_TRM × Fib_8, rho was 0.726789 in TCGA-BLCA, 0.595974 in GSE13507 and 0.750455 in GSE31684. For Mac_IFN × Fib_8, rho was 0.679069, 0.612981 and 0.708290, respectively. For Mac_TRM × Fib_7, rho was 0.822124, 0.584733 and 0.851213; for Mac_IFN × Fib_7, rho was 0.829429, 0.704590 and 0.806869. Each correlation had a bootstrap confidence interval excluding zero and a Benjamini–Hochberg-adjusted P value below 0.05.

The positive pattern was therefore reproducible as tissue-level covariance across the three cohorts. However, because all 12 observations from the locked 2 × 2 pair universe were positive, the data did not identify a unique pair-specific association. In particular, the results do not establish a Mac_TRM–Fib_8-specific axis, a cellular interaction, or a causal relationship.

### External single-cell transportability separates weak discrete-state matching from detectable within-lineage coherence

Both external scRNA-seq datasets retained myeloid/macrophage and fibroblast/stromal cells from all included tumor patients (9/9 in GSE222315 and 11/11 in GSE301651), supporting patient-wise within-lineage analyses (Figure 3A).

Unintegrated state-level matching was evaluated jointly by finite comparable genes, sign agreement, signed effect correlation and top-20 marker overlap (Figure 3B). In GSE222315, Mac_TRM had 5/28

same-direction genes, signed effect correlation 0.226400 and zero shared top-20 markers; Mac_IFN had 8/30, 0.106663 and zero shared markers; and Fib_8 had 5/30, 0.183436 and zero shared markers. Fib_7 matching was non-estimable where the source comparison had no finite comparable-gene effect correlation and was retained as NE/NA rather than reconstructed. In GSE301651, Mac_TRM had 3/28 same-direction genes, signed effect correlation 0.639349, one shared top-20 marker and Jaccard 0.025641; Mac_IFN had 4/30, 0.217730 and zero shared markers; and Fib_8 had 0/30, 0.454402 and zero shared markers. Fib_7 again remained NE/NA where non-estimable. Thus, a positive signed-effect correlation by itself did not constitute discrete-state rediscovery when direction agreement and marker overlap were weak; the Fib_8 GSE301651 result illustrates this distinction directly.

Harmony was examined as a sensitivity analysis, not as a parameter search. Dominant-patient fractions decreased after Harmony for every evaluated program-dataset combination, including Mac_TRM from 0.873779 to 0.520548 and Fib_8 from 0.670139 to 0.279621 in GSE222315, and Mac_TRM from 0.677193 to 0.508711 and Fib_8 from 0.407658 to 0.383954 in GSE301651. Matching metrics changed in mixed directions after Harmony, and top-20 marker overlap was not rescued (Figure 3C).

We next evaluated fixed-program coherence without requiring a matched cluster. Within each patient and the appropriate lineage, each gene was correlated across cells with the LOO score of the remaining comparable genes. Dataset-level median patient rho was positive for all four programs in both external datasets: Mac_TRM (0.059092 in GSE222315; 0.207955 in GSE301651), Mac_IFN (0.082008; 0.188597), Fib_8 (0.362596; 0.467400) and Fib_7 (0.146313; 0.090781) (Figure 3D). The q95 counts in Table 1 identify patients whose observed rho exceeded the 95th percentile of the corresponding matched-null distribution; they are not counts of rho-positive patients. These results describe detectable within-lineage coherence of fixed gene sets and do not validate discrete states.

Expression-matched null testing supported this descriptive coherence result. Across the 80 patient-program observations, each observed median LOO rho exceeded the median of its patient-specific null distribution. The global median null rho was 0.000962. The dataset-level median null rho values were 0.007419, 0.000275, -0.005517 and -0.017162 in GSE222315 for Fib_7, Fib_8, Mac_IFN and Mac_TRM, respectively; and 0.008992, 0.003261, 0.004367 and -0.004568 in GSE301651. These locked V2 null summaries should not be interpreted as pooled cell-level significance tests.

**Table 1. Patient-wise LOO coherence and expression-matched null summaries.**

| Dataset | Program | Median observed rho | Median matched-null rho | Patients above matched-null 95th percentile |
|---|---|---|---|---|
| GSE222315 | Fib_7 | 0.146313 | 0.007419 | 8/9 |
| GSE222315 | Fib_8 | 0.362596 | 0.000275 | 9/9 |
| GSE222315 | Mac_IFN | 0.082008 | -0.005517 | 9/9 |
| GSE222315 | Mac_TRM | 0.059092 | -0.017162 | 9/9 |
| GSE301651 | Fib_7 | 0.090781 | 0.008992 | 10/11 |
| GSE301651 | Fib_8 | 0.467400 | 0.003261 | 11/11 |
| GSE301651 | Mac_IFN | 0.188597 | 0.004367 | 11/11 |
| GSE301651 | Mac_TRM | 0.207955 | -0.004568 | 11/11 |

The matched-null result supports coherence relative to the specified expression-matched null, not stable state identity or a mechanism.

**Program-gene sensitivity was limited in bulk scoring**

Across the three bulk platforms, rescoring on common genes changed the 12 locked pair-by-cohort correlations by no more than 0.020 in absolute value (Figure 4A). This result indicates that the reported bulk co-variation was not driven by platform-specific absence of individual program genes.

Two conservative locked gene-removal sensitivity analyses were also retained. For Mac_TRM × Fib_8, removal of CLEC9A, IL2RA, SLC12A5 and HLA-DQA2 was evaluated without redefining the program (Figure 4B). For the two Fib_7-containing pairs, removal of TYROBP, SRGN and LYZ was evaluated in the same fixed before-versus-after framework (Figure 4C). These analyses showed the effect of limited marker removal on bulk correlations, but they did not resolve the identity-confounded interpretation of Fib_7 or establish a discrete state.

**Tissue-composition adjustment substantially changes bulk correlations**

Fixed-marker adjustment substantially attenuated the Mac_TRM × Fib_8 and Mac_IFN × Fib_8 bulk associations (Figure 5A). Fully adjusted Mac_TRM × Fib_8 rho values were 0.594377, 0.313921 and 0.335700 in TCGA-BLCA, GSE13507 and GSE31684; the corresponding Mac_IFN × Fib_8 values were 0.073384, -0.064512 and -0.078580. The paired fixed-marker bootstrap compared the difference in fixed-marker-adjusted residual correlations for these two pairs within each cohort. The observed difference in fixed-marker-adjusted residual correlations was 0.520994 in TCGA-BLCA (bootstrap median 0.515163, 95% CI 0.405617–0.623064), 0.378434 in GSE13507 (median 0.370351, 95% CI 0.183882–0.547282), and 0.414280 in GSE31684 (median 0.391105, 95% CI 0.109902–0.666248) (Figure 5B). This comparison is a composition-sensitivity analysis and does not assign cellular causation.

Mac_TRM and Mac_IFN scores were strongly correlated with the fixed macrophage-abundance proxy: 0.895745, 0.658120 and 0.925219 for Mac_TRM, and 0.953167, 0.872335 and 0.964221 for Mac_IFN, in TCGA-BLCA, GSE13507 and GSE31684, respectively (Figure 5C). This collinearity limits interpretation of adjusted residual associations. The fixed-marker framework is approximate; the results show that estimated tissue composition materially affects the bulk correlations, not that a composition-independent association has been identified.

**Spatial within-section score co-variation is weak and technically sensitive**

Spatial analyses used 22 GSE319536 sections from 22 patients. Across the complete locked 2 x 2 pair universe, the existing section-level output evaluated all four pairs; depth-adjusted within-section correlations were positive in 22/22 sections for Mac_TRM x Fib_7, Mac_TRM x Fib_8 and Mac_IFN x Fib_7, and in 21/22 sections for Mac_IFN x Fib_8, while Figure 6 presents Mac_TRM x Fib_8 as a representative visualization. At the recoverable UMI threshold of 200, 85,347 spots were retained. The median raw Mac_TRM × Fib_8 within-section Spearman rho was 0.331259 and the median depth-adjusted rho was 0.196757 (Figure 6A). At UMI thresholds of 200, 500 and 1,000, the median depth-adjusted rho was 0.196757, 0.222349 and 0.248793, respectively; 22/22 sections were evaluable at each threshold (Figure 6B). The number of retained spots declined from 85,347 to 72,437 and 56,017 as the threshold increased.

Section-level Moran's I after QC was low, with program medians of approximately 0.051 for Fib_7, 0.042 for Fib_8, 0.047 for Mac_IFN and 0.059 for Mac_TRM (Figure 6C). Mac_TRM score detectability, defined by the historical descriptive threshold of a within-section 75th percentile greater than 0.2, was 0/22 at each assessed threshold. The spatial data therefore provided limited, technically sensitive evidence of within-section score co-variation; they did not establish co-localization, a niche, communication or a myeloid–fibroblast interaction.

**Clinical associations provide secondary phenotype context without prognostic utility**

Clinical comparisons were heterogeneous across cohorts. For Fib_8, associations included stage I–II versus III–IV in TCGA-BLCA (Cliff's delta = -0.372, BH-adjusted P = 5.8 × 10^-8), high versus low grade in TCGA-BLCA (Cliff's delta = +0.526, BH-adjusted P = 1.3 × 10^-4), muscle-invasive versus non-muscle-invasive disease in GSE13507 (Cliff's delta = +0.379, BH-adjusted P = 1.2 × 10^-4), grade in GSE13507 (Cliff's delta = +0.228, BH-adjusted P = 0.015), and T2 versus T3/T4 disease in GSE31684 (Cliff's delta = -0.414, BH-adjusted P = 0.012). Full multiplicity-adjusted results are provided in Supplementary Table S5. Mac_TRM phenotype associations were inconsistent across cohorts. No overall-survival association met the specified significance criterion. These findings provide secondary phenotype context only and do not support prognostic utility.

# Discussion

This study examined whether fixed single-cell-derived gene programs retained similar properties when measured in bulk tissue, external single-cell datasets and spatial transcriptomics. Molecular classifications of bladder cancer [26–28], stromal TGFβ-associated immune exclusion [29], and single-cell studies of tumor-infiltrating myeloid cells and cancer-associated fibroblasts [30–32] provide useful biological context, but they do not show whether a fixed program can be transported across datasets. Our results suggest that transportability depends on the representation level.

At the bulk-tissue level, all four eligible myeloid–stromal pairs were positively correlated across three cohorts. In two external scRNA-seq datasets, the fixed programs also showed patient-wise within-lineage coherence and performed above an expression-matched null. The discovery state-defining patterns, however, were only weakly reproduced by cluster/state-level matching. Spatial score co-variation was also weak after depth adjustment. The programs therefore appear to retain broad transcriptional and compositional signals across datasets, but we did not find strong evidence that the original discrete cell states were preserved.

The locked 2 × 2 pair universe is important here. Mac_TRM × Fib_8 was not tested as a single selected pair. All four combinations of the two myeloid-associated and two fibroblast/stromal-associated programs showed positive bulk correlations in all three cohorts. For this reason, the overall pattern matters more than the ranking of individual pairs. The bulk data support reproducible tissue-level myeloid–stromal co-variation, but they do not identify a unique program pair or a specific cellular axis. This is particularly relevant because bulk program scores can reflect several features of tissue composition.

The external scRNA-seq results help separate program coherence from discrete-state replication. Both external datasets had complete patient coverage at the major-lineage level, so the results were not driven by a lineage represented by only one donor. Even so, cluster matching showed limited sign retention and almost no top-20 marker overlap with the discovery programs. One example was GSE301651 Fib_8, where the signed effect-vector correlation was positive despite zero same-direction genes and no top-20 overlap. We do not think this is enough to call the state rediscovered. Harmony reduced dominant-patient fractions, but top-20 overlap remained poor. Other matching metrics changed in different directions. The overall interpretation was therefore unchanged after integration.

The cluster-free LOO analysis asked a simpler question. Within each patient and the relevant lineage, were genes from a fixed program still positively coordinated across cells after adjustment for technical covariates? Fib_8 showed the largest dataset-level median coherence. Mac_IFN and Mac_TRM were also positive relative to the matched null, although their effects were smaller. Dataset-level medians of the patient summaries were positive, and observed patient-program values were near the upper tail of the specified expression-matched null distributions. This supports within-lineage coherence of the fixed gene sets. It does not mean that the original discrete state was recovered. The patient, not the individual cell, remained the biological replication unit in these analyses.

The program-gene sensitivity analyses gave a similar result. Rescoring with genes shared across platforms changed none of the locked bulk correlations by more than 0.020. The bulk findings therefore did not depend strongly on genes missing from individual platforms. We also removed selected atypical Mac_TRM genes and selected Fib_7-associated genes to test whether a small number of markers were driving the results. These were sensitivity analyses only and did not redefine the programs. The Fib_7 analysis also does not resolve its identity-confounded status or show that the signal came from contamination, doublets or ambient RNA.

Composition had a much larger effect. Fixed-marker adjustment substantially reduced the bulk correlations, and the program scores were highly collinear with the macrophage-abundance proxy. The residual associations therefore depend on an approximate composition model and should not be described as composition-independent. In our view, the bulk results are most clearly interpreted as tissue-level co-variation.

The spatial results were weaker. Within-section correlations decreased after depth adjustment and varied with the UMI threshold. Section-level Moran's I was also low. The spatial data therefore provide only weak and technically sensitive evidence of within-section score co-variation. They do not support spatial co-localization or a defined cellular niche. The clinical analyses were secondary and varied across datasets and endpoints. No overall-survival association was significant, so these results do not support a prognostic claim.

# Limitations

Several limitations affect the interpretation of these results. The program inventory came from exploratory analyses, and representation of discovery samples was uneven. The cohorts and platforms were also heterogeneous, and some of the later transportability datasets were evaluated post-selection.

Complete major-lineage patient coverage in the external datasets does not mean that every discovery state was present or recoverable. The best-cluster signed-effect correlation is selection-conditioned because the maximum correlation was chosen across candidate clusters; accordingly, state rediscovery was interpreted descriptively and jointly with direction retention and top-20 marker overlap rather than as a formal independent hypothesis test. Fixed-marker composition adjustment was approximate and was affected by collinearity between program scores and the composition proxy. Spatial analyses were limited by spot mixing, sequencing depth and incomplete provenance of manual filtering.

The matched-null analysis also depends on how the expression-matched null was defined. It controls for external expression abundance under the same patient- and lineage-specific LOO procedure, but it does not reproduce every property introduced during discovery-stage marker ascertainment. These limitations do not support claims of validated cell subtypes, cellular interaction, mechanism, causal direction, composition independence, spatial co-localization or clinical utility.

## Conclusions

Transportability differed by representation level and program. The fixed programs showed reproducible covariance in bulk tissue and detectable within-lineage coherence in external single-cell datasets. The single-cell results, however, did not establish preservation of the original discrete states. We also found no evidence for a specific myeloid–stromal axis, cellular interaction, mechanism or clinical utility. Composition sensitivity and the weak, technically sensitive spatial results further limit the interpretation of these transported programs.

# Declarations

### Authors' Contributions

Mingran Zhang conceived the study, designed the methodology, performed the computational analyses, curated the data, prepared the figures, and wrote the original manuscript. You Zhao and Hongzhao reviewed and revised the manuscript. All authors reviewed and approved the final version of the manuscript.

### Funding
This work was supported by the Wannan Medical College Teaching Hospital Research Project (grant no. WK2024JXYY044), the Changzhou Longcheng Medical Star Recommendation Project for Young Medical Sci-Tech Talents (grant no. lcyx2025010), and the Science Foundation of Kangda College of Nanjing Medical University (grant no. KD2024KYJJ274).

### Ethical Approval and Accordance

Not applicable. This study consisted exclusively of secondary analyses of publicly available, de-identified datasets. No participants were prospectively recruited, no intervention was performed, and no identifiable human material was collected by the authors. Therefore, institutional ethical approval was not required for the present study.

### Consent to participate

Not applicable. The study used publicly available, de-identified datasets and involved no direct recruitment of identifiable participants.

### Availability of data and materials

All datasets analyzed in this study are publicly available. The primary single-cell discovery cohort GSE135337 is available from the NCBI Gene Expression Omnibus (GEO) at https://www.ncbi.nlm.nih.gov/geo/query/acc.cgi?acc=GSE135337. The single-cell/single-nucleus validation cohort GSE169379 is available at https://www.ncbi.nlm.nih.gov/geo/query/acc.cgi?acc=GSE169379. The external transportability cohorts GSE222315 and GSE301651 are available at https://www.ncbi.nlm.nih.gov/geo/query/acc.cgi?acc=GSE222315 and https://www.ncbi.nlm.nih.gov/geo/query/acc.cgi?acc=GSE301651, respectively. The spatial

transcriptomics dataset GSE319536 is available at https://www.ncbi.nlm.nih.gov/geo/query/acc.cgi?acc=GSE319536. The bulk transcriptomic cohorts GSE13507 and GSE31684 are available at https://www.ncbi.nlm.nih.gov/geo/query/acc.cgi?acc=GSE13507 and https://www.ncbi.nlm.nih.gov/geo/query/acc.cgi?acc=GSE31684, respectively. TCGA-BLCA data are publicly available through the NCI Genomic Data Commons at https://portal.gdc.cancer.gov/projects/TCGA-BLCA. Processed data and analysis materials generated for this study are available from Zenodo at https://doi.org/10.5281/zenodo.22761767.

**Acknowledgements**
Not applicable.

**Generative AI Disclosure**
ChatGPT and Codex (OpenAI) were used primarily as technical tools to assist with execution of predefined computational tasks, preparation of figures, organization and formatting of analysis outputs, and limited manuscript editing. All study design, dataset and method selection, statistical decisions, interpretation of results, and scientific conclusions were determined and verified by the authors. The authors take full responsibility for the accuracy and integrity of the submitted work.

**Competing Interests**
The authors declare no competing interests.

# References

1. Robertson AG, Kim J, Al-Ahmadie H et al. Comprehensive molecular characterization of muscle-invasive bladder cancer. Cell 2017, 171, 540–556.e25. https://doi.org/10.1016/j.cell.2017.09.007. PMID: 28988769.
2. Tran MA et al. A tumor-promoting inflammatory SPP1 + macrophage-IL-6-CRP axis drives immune dysfunction in bladder cancer. Cancer Discov. 2026, 16, 1126–1151. https://doi.org/10.1158/2159-8290.CD-25-1774. PMID: 41747249.
3. Liu S et al. Single-cell dissection of multifocal bladder cancer reveals malignant and immune cells variation between primary and recurrent tumor lesions. Commun. Biol. 2024, 7, 1659. https://doi.org/10.1038/s42003-024-07343-7. PMID: 39702554.
4. Chen Z, Zhou L, Liu L et al. Single-cell RNA sequencing highlights the role of inflammatory cancer-associated fibroblasts in bladder urothelial carcinoma. Nat. Commun. 2020, 11, 5077. https://doi.org/10.1038/s41467-020-18916-5. PMID: 33033240.
5. Lai H, Cheng X, Liu Q et al. Single-cell RNA sequencing reveals the epithelial cell heterogeneity and invasive subpopulation in human bladder cancer. Int. J. Cancer. 2021, 149, 2099–2115. https://doi.org/10.1002/ijc.33794. PMID: 34480339.
6. Chen H, Peng Y, Ji Z, Dong J. SPP1 + Macrophage-POSTN+ Fibroblast-Endothelial Triad Dictates Immunotherapy Response in Bladder Cancer. FASEB J. 2026, 40, e71546.

https://doi.org/10.1096/fj.202504456RR. PMID: 41653034.

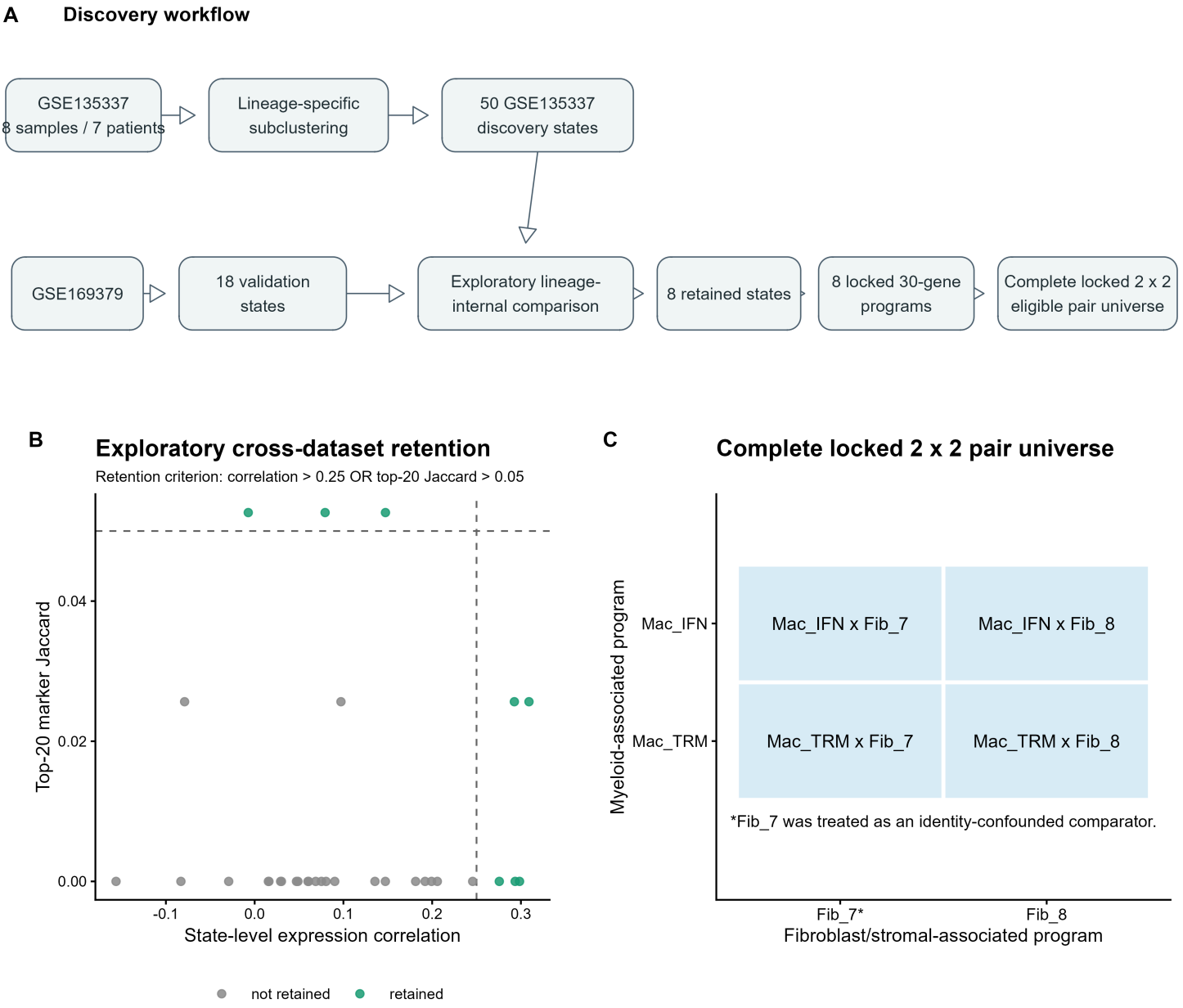
7. Nalio Ramos R et al. Tissue-resident FOLR2 + macrophages associate with CD8 + T cell infiltration in human breast cancer. Cell. 2022, 185, 1189–1207.e25. https://doi.org/10.1016/j.cell.2022.02.021. PMID: 35325594.
8. Guimaraes GR et al. Single-cell resolution characterization of myeloid-derived cell states with implication in cancer outcome. Nat. Commun. 2024, 15, 5694. https://doi.org/10.1038/s41467-024-49916-4. PMID: 38972873.
9. Zhao H et al. Prediction of prognosis and recurrence of bladder cancer by ECM-related genes. J. Immunol. Res. 2022, 2022, 1793005. https://doi.org/10.1155/2022/1793005. PMID: 35450397.
10. Yin H et al. Identification of a 13-mRNA signature for predicting disease progression and prognosis in patients with bladder cancer. Oncol. Rep. 2020, 43, 379–394. https://doi.org/10.3892/or.2019.7429. PMID: 31894276.
11. Kim WJ et al. Predictive value of progression-related gene classifier in primary non-muscle invasive bladder cancer. Mol. Cancer. 2010, 9, 3. https://doi.org/10.1186/1476-4598-9-3. PMID: 20059769.
12. Riester M et al. Combination of a novel gene expression signature with a clinical nomogram improves the prediction of survival in high-risk bladder cancer. Clin. Cancer Res. 2012, 18, 1323–1333. https://doi.org/10.1158/1078-0432.CCR-11-2271. PMID: 22228636.
13. Ståhl PL, Salmén F, Vickovic S et al. Visualization and analysis of gene expression in tissue sections by spatial transcriptomics. Science. 2016, 353, 78–82. https://doi.org/10.1126/science.aaf2403. PMID: 27365449.
14. Salmén F, Ståhl PL, Mollbrink A et al. Barcoded solid-phase RNA capture for Spatial Transcriptomics profiling in mammalian tissue sections. Nat. Protoc. 2018, 13, 2501–2534. https://doi.org/10.1038/s41596-018-0045-2. PMID: 30353172.
15. Andersson A, Bergenstråhle J, Asp M et al. Single-cell and spatial transcriptomics enables probabilistic inference of cell type topography. Commun. Biol. 2020, 3, 565. https://doi.org/10.1038/s42003-020-01247-y. PMID: 33037292.
16. Kleshchevnikov V, Shmatko A, Dann E et al. Cell2location maps fine-grained cell types in spatial transcriptomics. Nat. Biotechnol. 2022, 40, 661–671. https://doi.org/10.1038/s41587-021-01139-4. PMID: 35027729.
17. Marx V. Method of the Year: spatially resolved transcriptomics. Nat. Methods 2021, 18, 9–14. https://doi.org/10.1038/s41592-020-01033-y. PMID: 33408395.
18. Hao Y, Hao S, Andersen-Nissen E et al. Integrated analysis of multimodal single-cell data. Cell 2021, 184, 3573–3587.e29. https://doi.org/10.1016/j.cell.2021.04.048. PMID: 34062119.
19. Korsunsky I, Millard N, Fan J et al. Fast, sensitive and accurate integration of single-cell data with Harmony. Nat. Methods. 2019, 16, 1289–1296. https://doi.org/10.1038/s41592-019-0619-0. PMID: 31740819.
20. Newman AM, Steen CB, Liu CL et al. Determining cell type abundance and expression from bulk tissues with digital cytometry. Nat. Biotechnol. 2019, 37, 773–782. https://doi.org/10.1038/s41587-

019-0114-2. PMID: 31061481.

21. Aran D, Hu Z, Butte AJ. xCell: digitally portraying the tissue cellular heterogeneity landscape. Genome Biol. 2017, 18, 220. https://doi.org/10.1186/s13059-017-1349-1. PMID: 29141660.
22. Becht E, Giraldo NA, Lacroix L et al. Estimating the population abundance of tissue-infiltrating immune and stromal cell populations using gene expression. Genome Biol. 2016, 17, 218. https://doi.org/10.1186/s13059-016-1070-5. PMID: 27765066.
23. Yoshihara K, Shahmoradgoli M, Martínez E et al. Inferring tumour purity and stromal and immune cell admixture from expression data. Nat. Commun. 2013, 4, 2612. https://doi.org/10.1038/ncomms3612. PMID: 24113773.
24. Yu K, Chen J et al. A Spatial Atlas of Muscle-Invasive Bladder Cancer Reveals Lineage-Specific Vulnerabilities and Immune Architecture. Cancer Discov. 2026. https://doi.org/10.1158/2159-8290.CD-26-0099. PMID: 42126225.
25. Gouin KH, Ing III, Plummer N. An N-Cadherin 2 expressing epithelial cell subpopulation predicts response to surgery, chemotherapy and immunotherapy in bladder cancer. Nat Commun. 2021;12:4906. https://doi.org/10.1038/s41467-021-25103-7.
26. Kamoun A, de Reyniès A, Allory Y et al. A consensus molecular classification of muscle-invasive bladder cancer. Eur. Urol. 2020, 77, 420–433. https://doi.org/10.1016/j.eururo.2019.09.006. PMID: 31563503.
27. Sjödahl G, Lauss M, Lövgren K et al. A molecular taxonomy for urothelial carcinoma. Clin. Cancer Res. 2012, 18, 3377–3386. https://doi.org/10.1158/1078-0432.CCR-12-0077-T. PMID: 22553347.
28. Choi W, Porten S, Kim S et al. Identification of distinct basal and luminal subtypes of muscle-invasive bladder cancer with different sensitivities to frontline chemotherapy. Cancer Cell. 2014, 25, 152–165. https://doi.org/10.1016/j.ccr.2014.01.009. PMID: 24525232.
29. Mariathasan S, Turley SJ, Nickles D et al. TGFβ attenuates tumour response to PD-L1 blockade by contributing to exclusion of T cells. Nature. 2018, 554, 544–548. https://doi.org/10.1038/nature25501. PMID: 29443960.
30. Cheng S, Li Z, Gao R et al. A pan-cancer single-cell transcriptional atlas of tumor infiltrating myeloid cells. Cell 2021, 184, 792–809.e23. https://doi.org/10.1016/j.cell.2021.01.010. PMID: 33545035.
31. Lavie D, Ben-Shmuel A, Erez N, Scherz-Shouval R. Cancer-associated fibroblasts in the single-cell era. Nat. Cancer 2022, 3, 793–807. https://doi.org/10.1038/s43018-022-00411-z. PMID: 35883004.
32. Elyada E, Bolisetty M, Laise P et al. Cross-species single-cell analysis of pancreatic ductal adenocarcinoma reveals antigen-presenting cancer-associated fibroblasts. Cancer Discov. 2019, 9, 1102–1123. https://doi.org/10.1158/2159-8290.CD-19-0094. PMID: 31197017.

# Figures

**Figure 1 | Discovery framework and original sample structure**

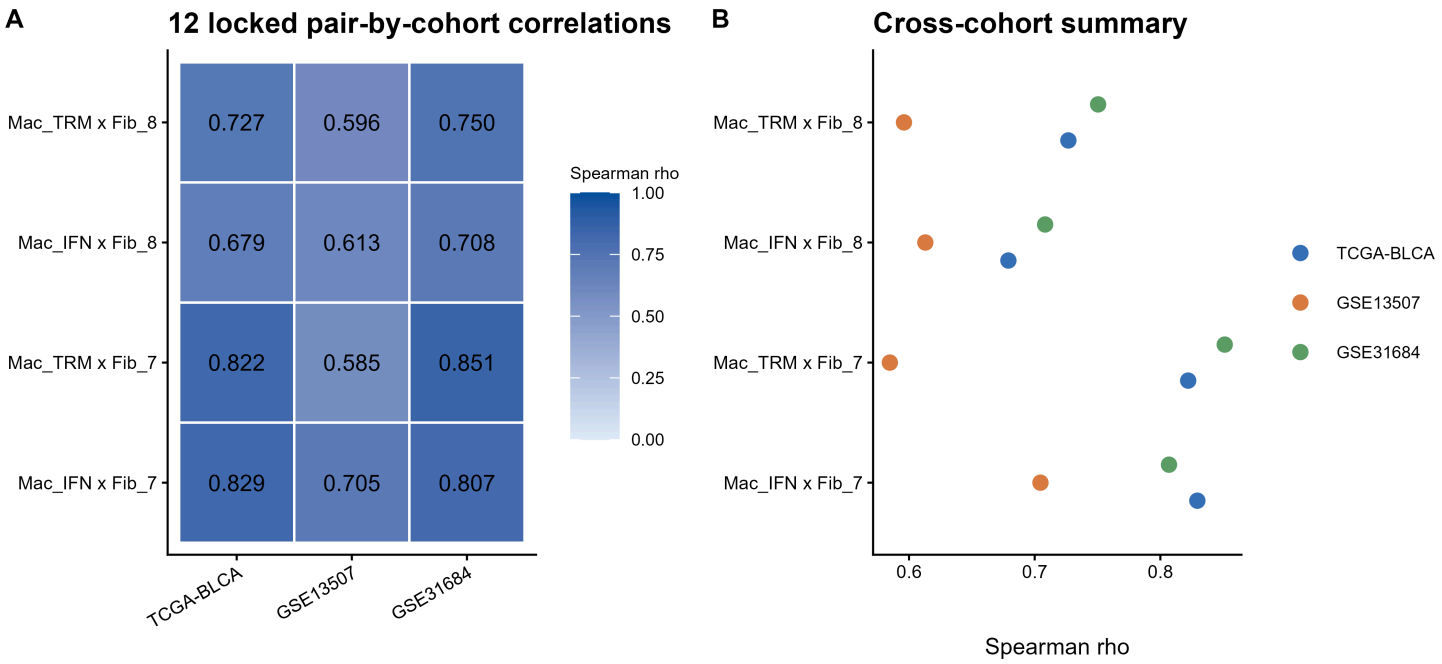



## Figure 1

Discovery framework and original sample structure.
(A) Discovery workflow from GSE135337 lineage-specific subclustering and state review to exploratory cross-dataset comparison with GSE169379, generation of eight locked 30-gene programs, and definition of the four programs used in the present analysis.
(B) Exploratory cross-dataset state retention based on expression correlation and top-20 marker Jaccard similarity; the retention criteria were correlation >0.25 or top-20 marker Jaccard >0.05.
(C) Complete locked 2 × 2 tested-pair universe comprising Mac_TRM and Mac_IFN crossed with Fib_7 and Fib_8.
GSE135337 contained 42,430 QC-retained cells from eight samples, and 50 discovery states were

evaluated using fixed state-QC rules. Program definitions were frozen before pair-level analysis; the pair-level focus was selected after program-level results in the evaluation cohorts had been inspected.

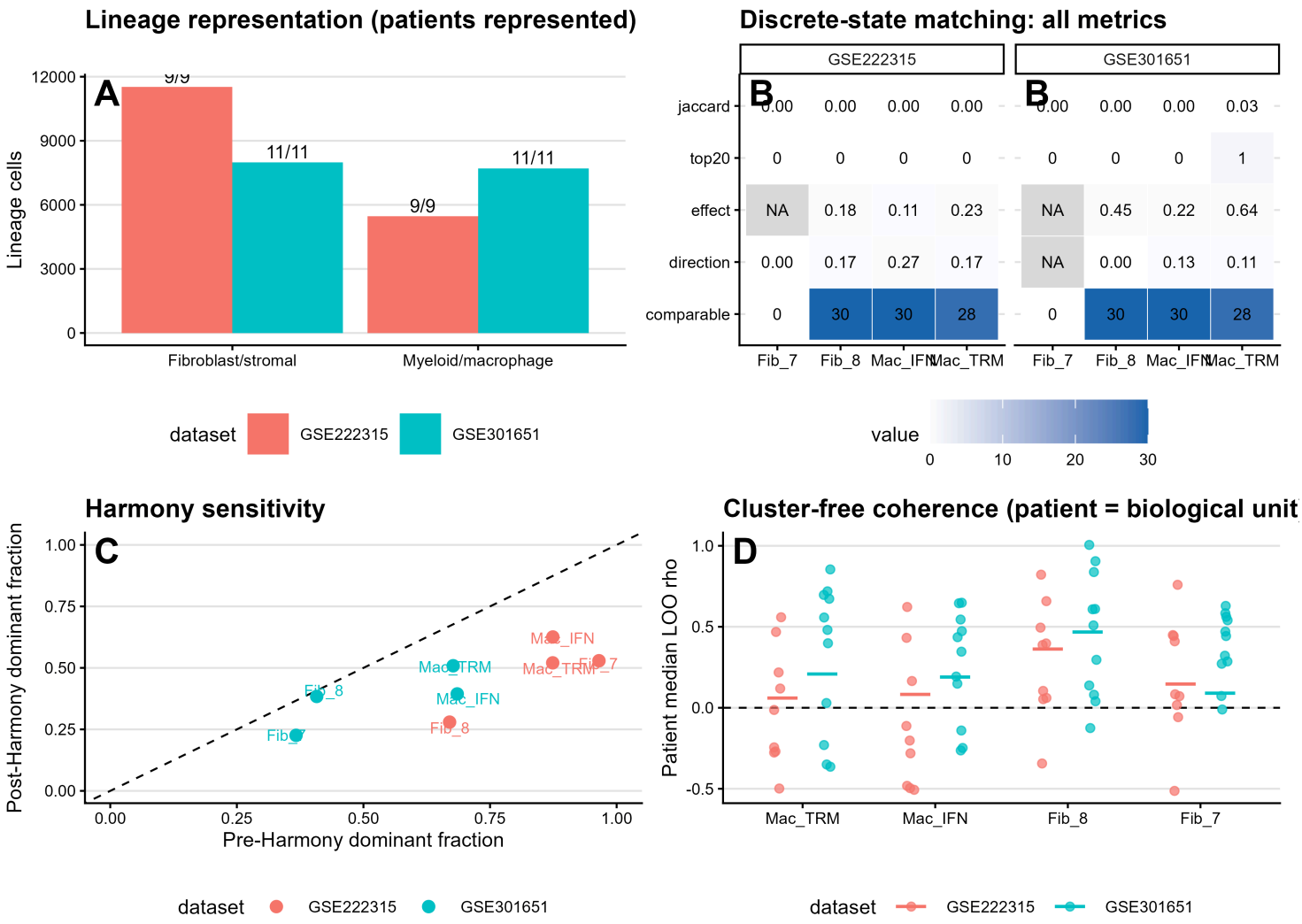
**Figure 2 | Bulk cross-cohort co-variation**




## Figure 2

Bulk cross-cohort transportability across the locked 2 × 2 pair universe.
(A) Heatmap of patient-level Spearman correlations for all four eligible myeloid–fibroblast/stromal pairs in TCGA-BLCA, GSE13507 and GSE31684.
(B) Cross-cohort summary of the same Spearman correlations for the four tested pairs. Fib_7 was retained as an identity-confounded comparator. The results are interpreted as tissue-level co-variation rather than evidence of a unique pair-specific interaction.

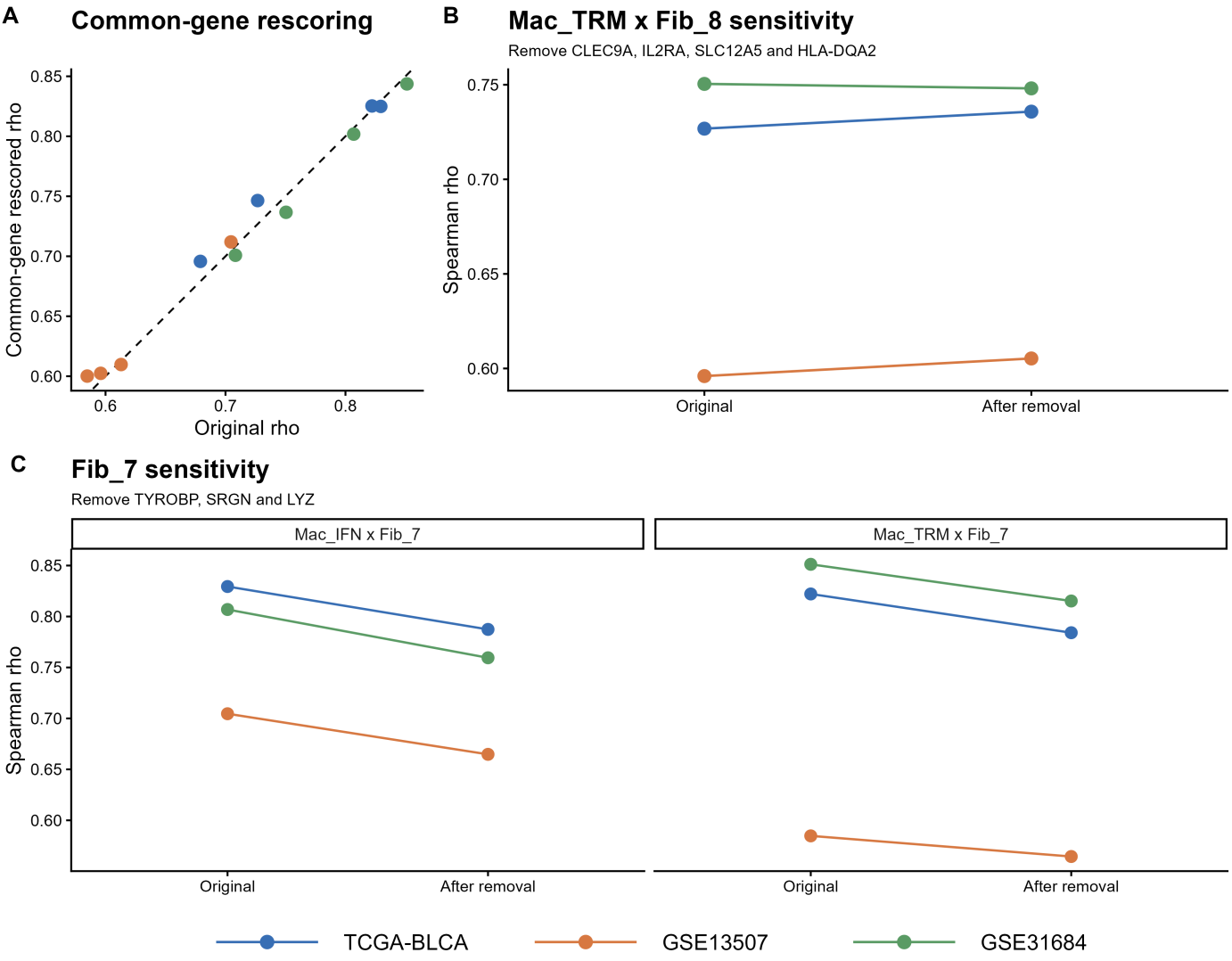
**Figure 3 | External single-cell transportability**




## Figure 3

External single-cell transportability.
(A) Myeloid/macrophage and fibroblast/stromal lineage representation and patient coverage in GSE222315 and GSE301651.
(B) Unintegrated discrete-state matching metrics, including comparable genes, same-direction fraction, signed-effect correlation, shared top-20 markers and top-20 Jaccard similarity; NE indicates not estimable.
(C) Harmony sensitivity showing dominant-patient fractions before and after patient-aware Harmony integration.
(D) Cluster-free patient-wise leave-one-gene-out coherence within the appropriate lineage. Individual points represent patient-level summaries and horizontal bars indicate dataset-level medians. Continuous gene-set coherence is descriptive and does not establish discrete cell-state identity.

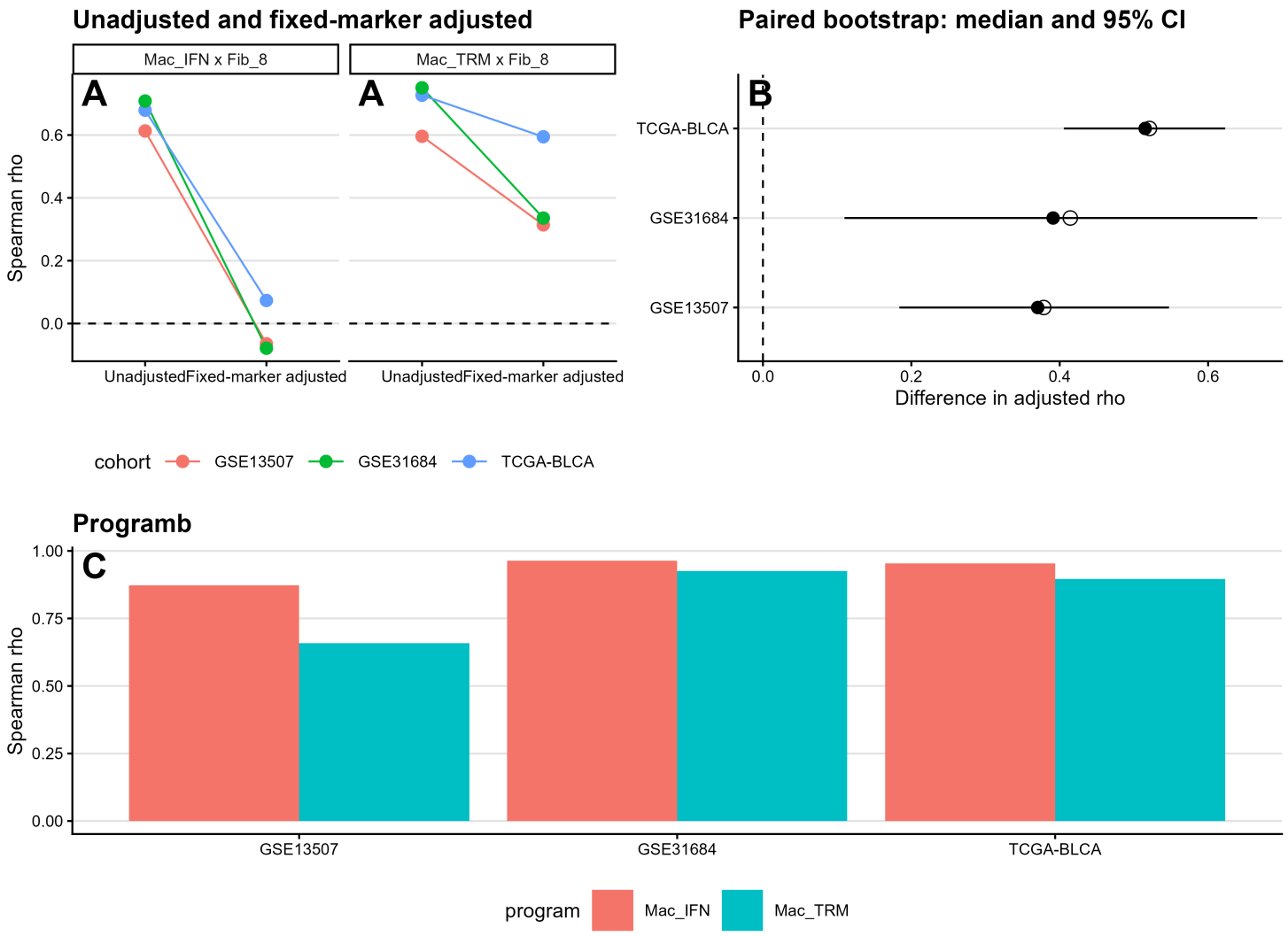
**Figure 4 | Program-definition robustness**




## Figure 4

Program-definition robustness.
(A) Common-gene rescoring sensitivity across the three bulk platforms.
(B) Mac_TRM × Fib_8 sensitivity after removal of the predefined atypical Mac_TRM genes CLEC9A, IL2RA, SLC12A5 and HLA-DQA2.
(C) Sensitivity of the Fib_7-containing pairs after removal of TYROBP, SRGN and LYZ from Fib_7. These analyses assess the robustness of the observed score associations without redefining the locked programs and do not establish discrete-state identity or a program-specific biological mechanism.

**Figure 5 | Tissue-composition sensitivity**




## Figure 5

Tissue-composition sensitivity.
(A) Unadjusted Spearman correlations and fixed-marker-adjusted residual correlations for Mac_TRM × Fib_8 and Mac_IFN × Fib_8 across TCGA-BLCA, GSE13507 and GSE31684.
(B) Paired-bootstrap comparison of the difference in fixed-marker-adjusted residual correlations, defined as rho(Mac_TRM × Fib_8) minus rho(Mac_IFN × Fib_8). Filled points indicate bootstrap medians, open points indicate observed differences, and horizontal lines indicate percentile 95% confidence intervals.
(C) Spearman correlations between Mac_TRM or Mac_IFN program scores and the fixed macrophage-abundance proxy in each bulk cohort. The fixed-marker framework is approximate, and program–proxy collinearity limits interpretation of residual associations.

**Figure 6 | Spatial within-section program co-variation**

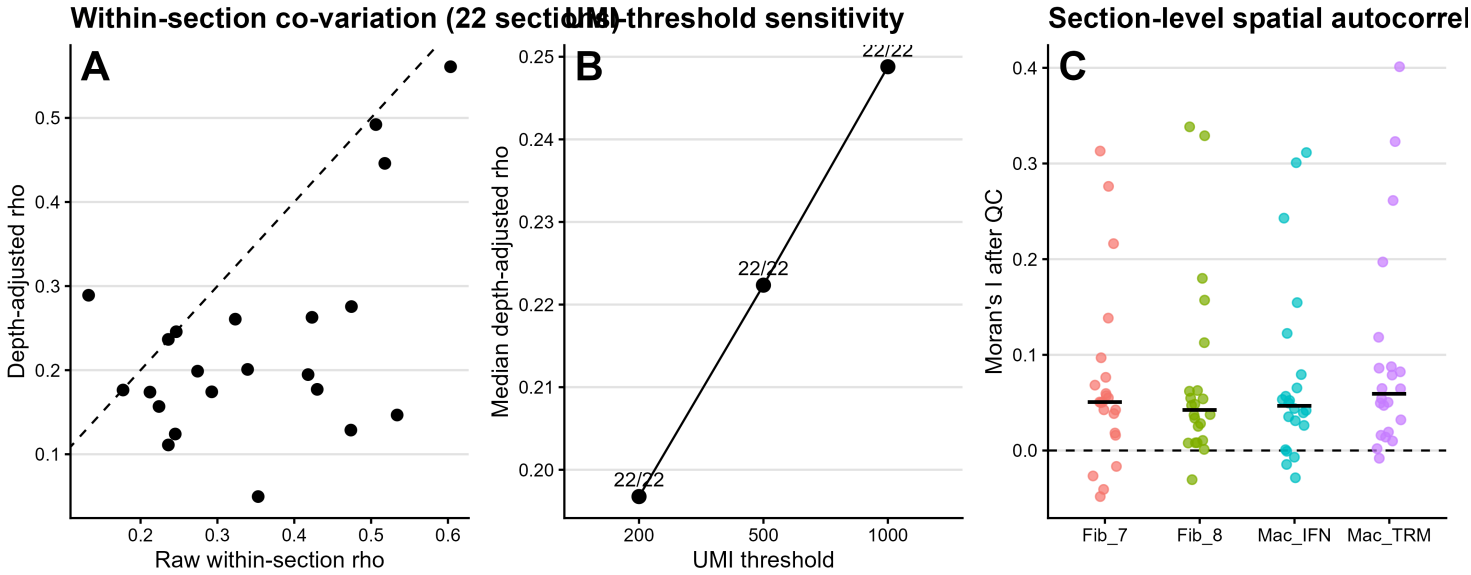



**Figure 6**

Spatial evidence.
(A) Raw versus depth/detection-adjusted within-section Spearman correlations for Mac_TRM × Fib_8 across 22 GSE319536 sections/patients; adjustment included total spot UMI and detected-gene count.
(B) UMI-threshold sensitivity of the median depth-adjusted within-section correlation at UMI thresholds of 200, 500 and 1,000; all 22 sections remained evaluable at each threshold.
(C) Section-level Moran's I after QC for Fib_7, Fib_8, Mac_IFN and Mac_TRM, with median values indicated. Spatial results are interpreted as weak, technically sensitive within-section score co-variation and not as co-localization, a niche or cellular communication.

# Supplementary Files

This is a list of supplementary files associated with this preprint. Click to download.

- SupplementaryTableS2.xlsx
- SupplementaryTableS5.xlsx
- SupplementaryTableS1.xlsx
- SupplementaryTableS3.xlsx
- SupplementaryTableS4.xlsx
- SupplementaryMaterials.docx